Available online at www.sciencedirect.com

SciVerse ScienceDirect

Ceramics International 39 (2013) 7179–7183

CERAMICS INTERNATIONAL

www.elsevier.com/locate/ceramint

Paper-derived hydroxyapatite

Steferson Luiz Stares[a,b,c,*], Márcio Celso Fredel[d], Peter Greil[a,b], Nahum Travitzky[a,b,*]

[a]Department of Materials Science and Engineering (Glass and Ceramics), University of Erlangen-Nuremberg, Erlangen, Germany
[b]Central Institute for New Materials and Processing Technology (ZMP), Fürth, Germany
[c]Biontech Degradable Polymers, Governador Celso Ramos, Brazil
[d]Departament of Mechanical Engineering, Federal University of Santa Catarina, Florianópolis, Brazil

Received 11 February 2013; received in revised form 18 February 2013; accepted 18 February 2013
Available online 26 February 2013

Abstract

Porous hydroxyapatite structures were manufactured via a novel preceramic paper process. Preceramic paper sheets were produced from aqueous suspensions loaded with different contents of pulp fiber and HA filler. Pressure loading was applied in order to increase the packing density in the paper sheets. The paper sheets were sintered at 1250 °C for 1 h. The porous ceramic specimens were characterized for density, porosity, microstructure and mechanical properties. A pronounced volumetric shrinkage was observed, but no surface flaws or inhomogeneous areas were detected. The mechanical strength using the ball on three balls test (B3B test) and elastic modulus of sintered specimens vary between 18 and 28 MPa and 0.65–1.53 GPa, respectively.

Keywords: Bioceramic; Preceramic paper; Hydroxyapatite; Bone tissue

1. Introduction

Recently a preceramic paper processing approach was used for the manufacturing of ceramic components. The process can be used to create a wide variety of shapes with tailored macro- and micro-scopic porosities for a broad field of applications [1–6]. Preceramic paper is made up of inorganic fibers and loaded with inorganic powders [7]. The processing approach used for the deposition of fibers or their mixtures with or without the addition of fillers defines the paper properties [1]. The organic fraction of the paper substrate is burned out during firing in air, leaving a porous ceramic residue [8].

In the present work, a novel preceramic paper derived hydroxyapatite has been developed with the goal of fabricating porous structures for use in bone reconstruction surgery. Paper web formation, sintering behavior and microstructure were studied as well as the strength and elastic modulus. In order to increase packing density in the sintered ceramic product, the effect of pressure on the paper properties was also studied.

2. Experimental

2.1. Preparation of preceramic paper

Preceramic papers loaded with hydroxyapatite spheres (HA) and pulp fibers were prepared from dilute aqueous suspensions. HA ($Ca_{10}(PO_4)_6(OH)_2$) spheres were obtained from Merck, Darmstadt, Germany, with a mean particle size of 4 μm and density of 3.15 g cm^{-3}. The aqueous suspension of a pulp mixture containing 0.30 wt% non-refined softwood pulp (Celbi PP, Celulose Beira Industrial (Celbi) S.A, Figueira da Foz, Portugal) with an average diameter of 15 μm and an average length of 657 μm was homogenized by vigorous stirring at a pH = 7.6 for 1 h. Solid retention was obtained by flocculation in the feedstock suspension, induced by addition of 8.0 vol% anionic starch ester (Fibraffin A5, Südstärke GmbH, Schrobenhausen, Germany).

Preceramic paper sheets were formed on a Rapid Köthen sheet forming device (Haage Laborblattbildner

*Correspondence to: Martensstr. 5, D-91058 - Erlangen, Germany. Tel.: +49 913185 28775; fax: +49 913185 28311.
E-mail addresses: slstares@hotmail.com (S.L. Stares), nahum.travitzky@ww.uni-erlangen.de (N. Travitzky).

0272-8842/$ - see front matter © 2013 Elsevier Ltd and Techna Group S.r.l. All rights reserved.
http://dx.doi.org/10.1016/j.ceramint.2013.02.062

Table 1
Feedstock composition for preceramic paper processing.

Specimen	Pulp fibers [vol%]	HA [vol%]	Starch [vol%]
A	42	50	8
B	32	60	8
C	22	70	8

BBS-2, Estanit GmbH, Mühlheim an der Ruhr, Germany). Compressed air was used for the agitation of the diluted stock. Circular sheets with a diameter of 200 mm were obtained after dewatering under mild vacuum ($<10^4$ Pa). The as-filtrated specimens were dried at 93 °C for 15 min resulting in preceramic paper sheets denoted "*as-fabricated*" series A, B, and C. Table 1 summarizes the feedstock composition excluding water.

In order to increase the packing density in the paper sheets, one group of the dried specimens was loaded in a calender device (CA 5/250-150-20, Sumet Messtechnik, Denklingen, Germany) applying a load of 40 N mm^{-1} and a temperature of 70 °C for a speed of 0.5 m min^{-1}. These samples are denoted "*pre-consolidated*". For both groups all dimensional variables were measured after drying and storing for 24 h at room temperature to account for relaxation and moisture regain.

The preceramic paper sheets were sintered in air atmosphere in an electrically heated furnace (HT 16/17, Nabertherm, Lilienthal, Germany). A single step annealing sequence was applied where the temperature was raised with a constant heating rate of 5 °C min^{-1} up to 200 °C, followed by a heating rate of 1 °C min^{-1} up to 450 °C. Temperature was held at 450 °C for 2 h followed by subsequent heating to 600 °C at 1 °C min^{-1} to allow complete removal of pulp fibers and paper aid chemicals. The sheets were finally sintered at 1250 °C for 1 h. Heating from 600 to 1250 °C and cooling were set to 5 °C min^{-1}. *In-plane* (parallel to the sample) as well as *out-of-plane* (perpendicular to the sample plane) sintering shrinkage was measured by a digital dial indicator with a resolution of 1 μm.

2.2. Characterization of samples

The apparent density of the samples (ρ_{ap}) was determined from weight and volume measurements. The thickness of the samples was measured with a digital dial indicator. Skeletal density ($\rho_{skeletal}$) of the samples was measured by He-Pycnometry (AccuPyc 1330, Micromeritics Instrument Corporation, Norcross, GA, USA). Total porosity of the samples (P_p) was derived from fractional densities ρ^* according to the equation

$$P_p = 1-\rho^* = 1-\frac{\rho_{ap}}{\rho_{skeletal}} \quad (1)$$

The microstructure of the preceramic papers was derived from SEM micrographs (ESEM, Quanta 200, FEI, Czech Republic).

2.3. Measurement of mechanical properties

The strength of the sintered ceramic specimens was measured using the ball on three balls test (B3B test) which permits testing of thin as-sintered specimens and allows easy specimen preparation as stresses at sample edges are absent [9]. Sample disks with a diameter of 4.8 mm were cut with a Nd:YAG-laser with a wavelength of 1064 nm and 100 W power (SMP065, Rofin-Sinar Laser GmbH, Bergkirchen/Gründing, Germany). A constant crosshead speed of 0.5 mm min^{-1} was applied (Instron 5565, Instron Corp., Canton, MA, USA). The load was applied perpendicularly on the top surface x–y and the failure load was taken as the peak load. The maximum tensile stress σ_{max} was calculated according to the equation

$$\sigma_{max} = \frac{F}{t^2}\left[c_0 + \frac{c_1 + c_2(t/R) + c_3(t/R)^2 + c_4(t/R)^3}{1 + c_5(t/R)}\left(1 + c_6\frac{R}{R_a}\right)\right] \quad (2)$$

where F is the maximum force at fracture, t the specimen thickness, R the disk radius ($R=2.40$ mm), R_a the support radius ($R_a=1.83$ mm), v the Poisson constant ($v=0.2$), and c_i refers to fitting factors for the geometrical correction term ($c_0=-12.354$, $c_1=15.549$, $c_2=489.2$, $c_3=-78.707$, $c_4=52.216$, $c_5=36.554$ and $c_6=0.082$).

Young's modulus of the sintered ceramic specimens was derived from the load–displacement curves obtained from 3-point-bar-bending experiments (5×30 mm^2, 20 mm bearing distance) applying a constant crosshead velocity of 0.5 mm min^{-1}. By calculating Young's modulus the contribution of the testing machine was taken into account. The mean value of the mechanical properties was derived from a minimum of 10 samples of each type of paper-derived ceramic at a temperature of 20 °C and a relative humidity of 28%.

3. Results and discussion

3.1. As-fabricated paper

In this work, a solid retention of 80–84 wt% was obtained by flocculation in the feedstock suspension. The properties of *as-fabricated* paper such as thickness, porosity, and density were strongly dependent on the fiber and filler content. Table 2 summarizes the main properties of the preceramic papers produced.

Paper of composition A showed the lowest values of apparent density (ρ_{ap}) (0.60 g cm^{-3}), open porosity (72%) and thickness (403 ± 16 μm). On the other hand, composition C presented the highest values of apparent density (0.67 g cm^{-3}), open porosity (75%) and thickness (410 ± 19 μm). Since the density of filler (3.15 g cm^{-3})

was higher than that of the fiber (1.58 g cm^{-3}), paper density increases with increase in filler content at constant volume [10]. Similarly, the filler distribution in the fiber network depends on filler properties, the fiber network and papermaking conditions. However, with increase in the filler content, the fiber network expands, resulting in increased thickness and porosity [11].

Fig. 1 shows representative images of the microstructure of the HA-loaded preceramic paper after the sheet-forming process for two principal orientations. The HA filler particles are homogeneously distributed between the cellulose fibers. While the fibers in the x–y plane only reveal a low degree of preferential orientation, the fibers are highly oriented perpendicular to the z direction.

Table 2
Properties of the *as-fabricated* preceramic papers.

Specimen	Open porosity [vol%]	Thickness [μm]	Apparent density [g cm^{-3}]
A	72	403 ± 16	0.60 ± 0.02
B	73	404 ± 12	0.65 ± 0.01
C	75	410 ± 19	0.67 ± 0.01

3.2. Pre-consolidated papers

The combined actions of heat and pressure promoted permanent deformations in the *pre-consolidated* papers. The porosity of the paper web determines a number of properties including permeability, elastic modulus, deformability and mechanical behavior. The porosity is determined by the packing characteristics of fibers, filler powders, chemical additives and processing conditions. A common belief is that paper compression occurs in the pores of the network while fibers are essentially incompressible [12]. As might be expected with pressure, a reduction in paper thickness as well as porosity was observed which indicates an increase of packing density in the paper web. Fig. 2 shows the influence of the compressive pressure on the apparent density and the open porosity of papers A, B and C. Pressure applied on the *as-fabricated* paper sheet resulted in a reduction of the paper sheet thickness of 37–39% and open porosity of 19–20%. On the other hand, the apparent density increase of 36–37% was measured.

3.3. Sintering behavior

Conversion of the preceramic paper preform into a ceramic product involves removal of the bio-organic pulp

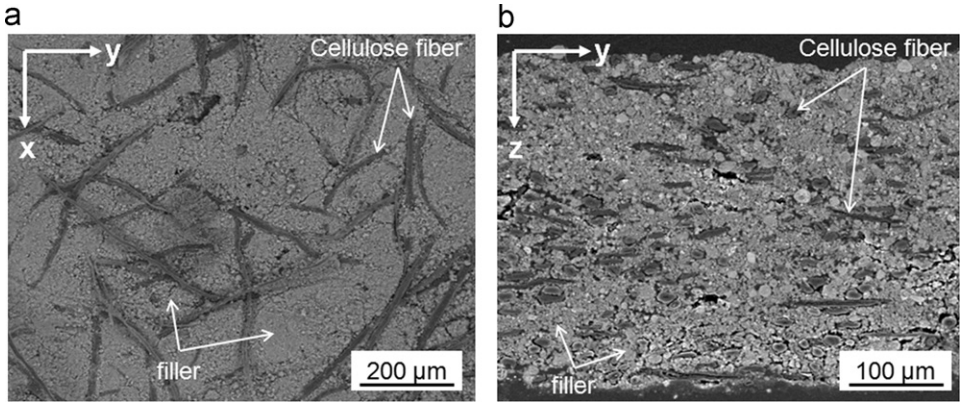

Fig. 1. SEM micrographs of a preceramic paper loaded with 70 vol% HA filler: (a) top surface view and (b) cross-sectional view.

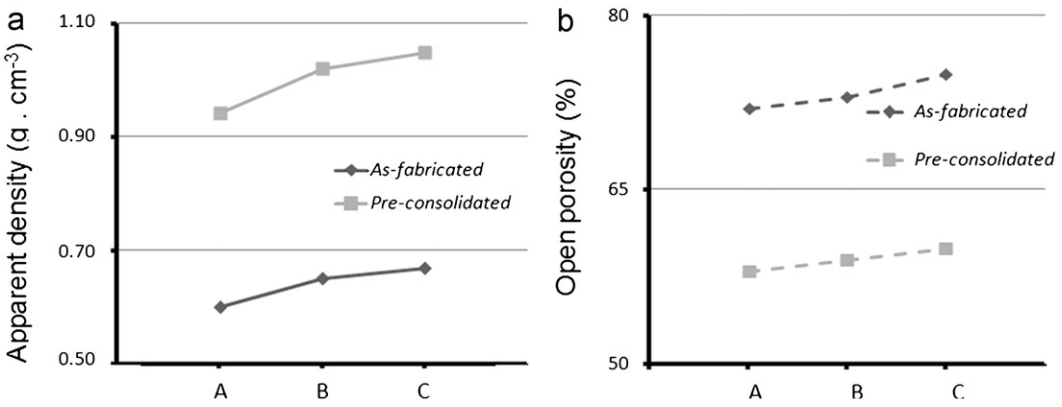

Fig. 2. Apparent density (a) and open porosity (b) of papers produced.

fibers and consolidation of the inorganic filler powder compact. Oxide ceramics are formed by annealing an oxide-filled preceramic paper preform in air to decompose and oxidize the fibers at temperatures above 300 °C, followed by sintering up to 1250 °C for 1 h [1]. This heat treatment led to the considerable shrinkage of the specimen. In all specimens, the in-plane shrinkage along the *x*- and *y*-directions ranged from 27% to 33%, and values shrinkage in the *z*-direction was significantly lower (2–6%). Anisotropic shrinkage variation has mainly been associated with spatial variation of powder packing density, the orientation of the pore/solid interface, the alignment of anisotropic particles, and the introduction of joining and bonding interfaces in multilayer packages [13–15]. The open porosities of the sheet specimens after sintering were 51–56% (*as-fabricated*) and 42–57% (*pre-consolidated*), and the apparent densities were 0.94–1.37 g cm^{-3} and 1.30–1.59 g cm^{-3}, respectively. During sintering in air atmosphere the bio-organic pulp fibers decompose leaving pores with a morphology, distribution, and orientation given by the pulp fibers template [1] (Fig. 3). These pores could not be removed during sintering. With increasing degree of filler content the packing density of preceramic paper was increased; however, a higher volume fraction of porosity was observed in the sintered ceramic sheet as well. Similarly the pressing of the paper sheets gave rise to a substantial reduction of porosity both in the green paper preform as well as in the sintered specimens.

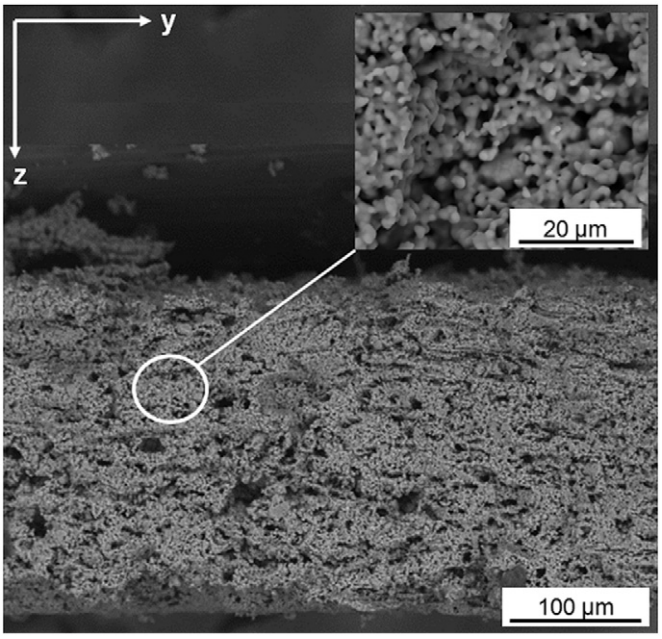

Fig. 3. Sintered paper-derived hydroxyapatite.

3.4. Mechanical properties

Fig. 4a shows the variation of strength for *as-fabricated* and *pre-consolidated paper samples*. Strength ranged from 18.14 ± 0.75 to 28.05 ± 0.70 MPa. As discussed above, increasing of HA content resulted in higher porosity of specimens. As expected, an increase in porosity resulted in decrease of the strength after sintering [16]. Similarly, pressing of the samples prior to heat treatments gave rise to a substantial reduction of porosity both in the paper sheets preform as well as in the sintered specimens. Applying pressure to the specimens resulted in a pronounced reduction of porosity in the sintered product and an increase in strength.

Fig. 4b shows the variation of Young's modulus from 0.65 ± 0.08 to 1.53 ± 0.13 GPa. An increase of porosity in the specimen also results in the reduction of Young's modulus. The strength and elastic modulus values of the sintered specimens are similar to that of human trabecular bone [17]. The combination of microstructures and mechanical strength of the specimens studied in this work showed a high potential for the use of preceramic paper process in the fabrication of materials for bone replacement applications such as fabricating scaffolds to repair trabecular defects. Bone tissue scaffold should possess an interconnected porous structure, with porosity $> 90\%$, pore size in the range 10–500 μm and values of mechanical strength at the range of the bone in question (e.g., for trabecular bone: failure strength of 7.6–20.7 MPa and Young's modulus of 0.05–0.5 GPa) [18,19]. The sintered specimens developed in the present work showed strength

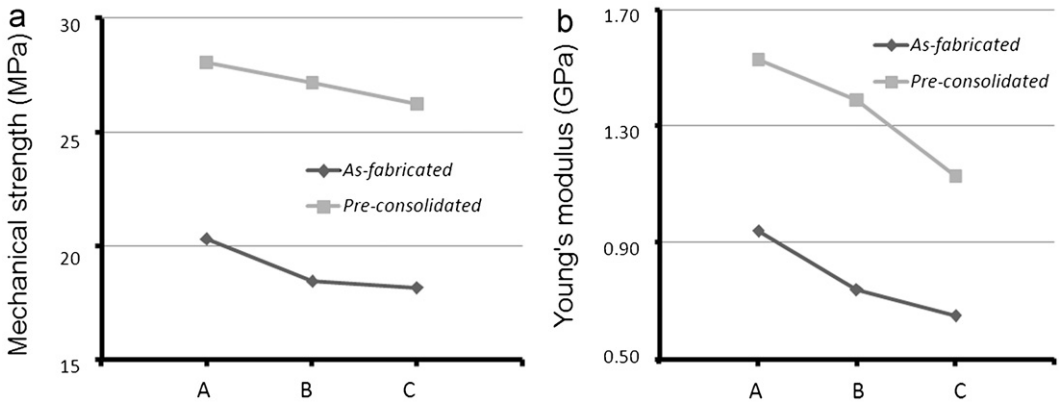

Fig. 4. (a) Strength and (b) Young's modulus of paper-derived hydroxyapatite.

from 18 to 28 MPa and Young's modulus from 0.65 to 1.53 GPa, which met the requirements mentioned above.

4. Conclusions

In the present work, a hydroxyapatite-loaded paper was fabricated for use in bone reconstruction. Applying compressive pressure improved paper consolidation and reduced thickness and porosity, which ultimately led to improved mechanical properties of the sintered paper products. The properties of final product were compatible with trabecular bone tissue.

Acknowledgments

The authors gratefully acknowledge support from the CAPES Foundation—Brazil (Scholarship Process no. 0618/11-0) and the German Science Foundation (DFG), Contract no. TR 250/4-1.

References

[1] N. Travitzky, H. Windsheimer, T. Fey, P. Greil, Preceramic paper-derived ceramics, Journal of the American Ceramic Society 91 (2008) 3477–3492.
[2] L. Weisensel, N. Travitzky, H. Sieber, P. Greil, Laminated object manufacturing (LOM) of Si–SiC composite, Advanced Engineering Materials 6 (2004) 899–903.
[3] H. Windsheimer, N. Travitzky, A. Hofenauer, P. Greil, Laminated object manufacturing of preceramic-paper-derived Si–SiC composites, Advanced Materials 19 (2007) 4515–4519.
[4] C.M. Gomes, A.P.N. Oliveira, D. Hotza, N. Travitzky, P. Greil, LZSA glass–ceramic laminates: fabrication and mechanical properties, Journal of Materials Processing Technology 206 (2008) 194–201.
[5] B. Gutbrod, D. Haas, N. Travitzky, P. Greil, Preceramic paper derived alumina/zirconia ceramics, Advanced Engineering Materials 13 (2011) 494–501.
[6] S.L. Stares, A. Kirilenko, M.C. Fredel, P. Greil, L. Wondraczek, N. Travitzky, Paper-derived bioactive glass tape, Advanced Engineering Materials (2012)http://dx.doi.org/10.1002/adem.201200192.
[7] K.V. Breitveit, E.A. Chaikina, Heat-resistant insulating papers based on inorganic fibers, Elektrotechnika 5 (1972) 22–24.
[8] S. Dasgupta, S.K. Das, Paper pulp waste—a new source of raw material for the synthesis of a porous ceramic composite, Bulletin of Materials Science 25 (2002) 381–385.
[9] R. Danzer, P. Supancic, W. Harrer, Biaxial tensile strength test for brittle rectangular plates, Journal of the Ceramic Society of Japan 114 (2006) 1054–1060.
[10] K. Niskanen, Paper physics, in: finnish paper engineers association (Ed.), Papermaking Science and Technology, Gemmerus, Helsinki, 2008, pp. 20–26.
[11] R. Bown, The effect of particle size and shape of paper fillers on paper properties, Wochenblatt für Papierfabrikation 111 (1983) 737–740.
[12] J.A. Bristow, The paper surface in relation to the network, in: J.A. Bristow, P. Kolseth (Eds.), Paper—Structure and Properties, Marcel Dekker Inc., New York, 1986, pp. 169–182.
[13] H.A. Exner, E.A. Geiss, Anisotropic shrinkage of cordierite-type glass powder cilindrical compacts, Journal of Materials Research 3 (1988) 122–125.
[14] P.M. Raj, W.R. Cannon, Anisotropic shrinkage in tape-cast alumina: role of processing parameters and particle shape, Journal of the American Ceramic Society 82 (1999) 2619–2625.
[15] Y.C. Lin, J.H. Jean, Constrained densification kinetics of alumina/borosilicate glass plus alumina/alumina sandwich structure, Journal of the American Ceramic Society 85 (2002) 150–154.
[16] K. Rezwan, Q.Z. Chen, J.J. Blaker, A.R. Boccaccini, Biodegradable and bioactive porous polymer/inorganic composite scaffolds for bone tissue engineering, Biomaterials 27 (2006) 3413–3431.
[17] K.C.R. Kolan, M.C. Leu, G.E. Hilmas, R.F. Brown, M. Velez, Fabrication of 13-93 bioactive glass scaffolds for bone tissue engineering using indirect selective laser sintering, Biofabrication 3 (2011) 025004.
[18] S.J. Kaplan, W.C. Hayes, J.L. Stone, G.S. Beaupré, Tensile strength of bovine trabecular bone, Journal of Biomechanics 18 (1985) 723–727.
[19] J.L. Stone, G.S. Beaupre, W.C. Hayes, Multiaxial strength characteristics of trabecular bone, Journal of Biomechanics 16 (1983) 743–752.